

The role of metastability in enhancing water-oxidation activity

Nathalie Vonrüti and Ulrich Aschauer*

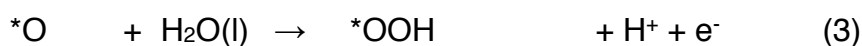
Department of Chemistry and Biochemistry, University of Bern, Freiestrasse 3, CH-3012 Bern, Switzerland

*Corresponding author: ulrich.aschauer@dcb.unibe.ch

While metastability enhanced water-oxidation activity was experimentally reported, the reason behind this effect is still unclear. We determine here, using density functional theory calculations, oxygen evolution reaction overpotentials for a variety of defective (001) surfaces of three different perovskite materials. For all three, we find a large range of overpotentials for different reaction sites including also overpotentials at the top of the activity volcano. Assuming that these sites dominate the apparent catalytic activity, this implies that a large number of geometrically different reaction sites, as they occur when a catalyst is operated at the border of its stability conditions, can lead to a strong enhancement of the apparent activity.

Introduction

Hydrogen fuel production by (photo)electrochemical water splitting has been intensively studied as a route to convert electrical or solar energy to chemical energy. The bottleneck in (photo)electrochemical water splitting is the oxygen evolution reaction (OER) for which previous studies of metal¹ and oxide² catalysts determined the OER reaction mechanism to consist of four consecutive proton-coupled one-electron transfer (PCET) steps with reaction intermediates *OH, *O and *OOH as shown in equations 1-4.



Several experimental studies found an inverse correlation between the activity and the stability of catalyst materials for the OER. Markovic and co-workers investigated activity-stability trends of the OER for crystalline and amorphous RuO₂^{3,4} as well as for different surface orientations of the perovskite SrRuO₃⁵. Based on the concentration of dissolved metal ions, they found a higher activity for less stable surfaces of both materials and concluded that a highly active OER catalyst should balance activity and stability. A mechanistic understanding of a catalyst's stability in enhancing the OER activity is however still elusive and actively debated. It was suggested that the OER activity is controlled by the density of surface defects rather than by the binding energy of the reaction intermediates on the perfect surface and that it may be linked to changes in oxidation state of Ru ions close to defects⁵. A very

recent study on RuO₂ thin films did, however, not find such a fundamental relationship between a material's stability and its activity⁶. While a correlation between the dissolution and the activity for different surface orientations was initially observed, it was also shown that the active OER sites are decoupled from the fastest-corroding Ru sites⁶.

To fully understand the activity-stability relationship one would ideally study the OER on specific reaction sites of defective materials. Experimentally it is, however, very challenging to characterize the geometry and activity of specific reaction sites since spectroscopic methods probe the average state of a catalyst. Computationally, one could readily calculate the overpotential and hence the activity of a given reaction site with a specific local geometry, but there exists no well-established method to determine the surface structure of a material with a low stability under OER conditions. For materials with a thermodynamically stable bulk, reasonable surface structures can be determined from the surface energy as a function of the applied potential and the pH by means of so-called surface Pourbaix diagrams (SPD)⁷. For thermodynamically unstable materials, on the other hand, one can only investigate the stability of the bulk with respect to competing phases^{8,9}, but a SPD would yield the surface with the minimal number of atoms as most stable, indicating that the thermodynamic equilibrium is the fully dissolved state. Nevertheless, in practice the dissolution may be kinetically slow and still allow these materials to be used as catalysts⁸. We refer here to such materials, that are thermodynamically unstable under OER conditions and for which we therefore cannot determine their surface structure by means of SPDs, as *metastable* materials.

The aim of the present work is to obtain a density functional theory (DFT) description of the OER on surfaces of metastable materials and to reveal how metastability can increase the performance of a catalyst. Computational studies on different oxides have, so far, mainly compared the OER activity of ideal stoichiometric, clean¹⁰ or adsorbate-covered¹¹, low-index surfaces which are unlikely to be good approximations for surfaces of a metastable material that may slowly dissolve under OER conditions⁸. Few studies reported the theoretical activity for reaction sites in the vicinity of point defects, steps or kinks^{7,12,13}, however without linking such structures to metastability. Our approach to account for metastability is to study the OER on a large variety of different reaction sites by sampling many defective surface structures, that should be representative for a slowly dissolving metastable material. We study the effect of metastability on the OER for three chemically very different perovskite structured catalysts, which enables us to distinguish between effects resulting from intrinsic material properties and effects of specific reaction sites. We compare LaTiO₂N (LTON) and SrRuO₃ (SRO), which differ by their d⁰ respectively d⁴ d-electron occupation and their insulating respectively metallic character. LTON is the best studied member of the family of perovskite oxynitrides that by virtue of their smaller band gap than oxides are considered promising photocatalysts¹⁴. Calculations¹⁵ and experimentally observed nitrogen loss¹⁶ indicate that LTON is metastable under OER conditions and SRO^{5,8} was also reported to be metastable. As these two materials differ not only in their metallic respectively insulating behaviour but also in their anion composition, we complement the set of materials with SrTiO₃ (STO), which shares properties with both LTON and SRO: like SRO it is a pure oxide but like LTON it is a d⁰ insulator. Moreover,

it shares the same A and B site with SRO and LTON respectively but unlike the other two materials STO was not reported to be metastable.

Computational approach

For all three materials we investigate both the AO and BO₂ terminated (001) surface, assuming that for a metastable or unstable material both terminations will be exposed as dissolution proceeds. For the oxynitride we also have to consider the anion order, which is different in the surface and the bulk: LaTiO₂N assumes a *cis* anion order in the bulk to maximize the overlap between the N *2p* and the Ti *3d* orbitals¹⁷ but the (001) surface prefers a non-polar *trans* anion order¹⁸. We therefore perform calculation on the *trans* surface but to account for the metastability-induced dissolution of the thin *trans* layer¹⁹ also investigate the OER on a *cis* ordered surface. As we find no significant difference between the two anion orders regarding OER reaction free energies, we do however not distinguish between them in our results.

Our stoichiometric and clean surface slabs contain four surface cation sites and we create defective surfaces with between one and four nitrogen, titanium, ruthenium, lanthanum or strontium vacancies in the surface layer (see Figure 1a for an example). We do not explicitly consider oxygen vacancies, since these are unlikely to form under oxidizing OER conditions¹¹. Occasionally, during surface relaxation - in particular for high cation-vacancy concentrations - either O₂ or N₂ recombine and desorb. In these cases, we stop the calculation and remove the desorbed molecules before continuing the calculation, which can in effect lead to oxygen vacancies. Since potentials relevant for (photo)electrochemical water splitting often lead to formation of oxidising surface

species¹¹, we also cover surface metal sites with either zero or one monolayer of OH or O in top position in the case of Ti and Ru as well as in the bridge position for La and Sr (see figure 1a, S1 and S2 for examples of different surface structures). For these surfaces we calculate the OER free energy profile on symmetrically inequivalent titanium, ruthenium, lanthanum and strontium reaction sites in the topmost formula-unit layer - meaning that for example on a defective BO₂ terminated surface also an A atom could become the reaction site.

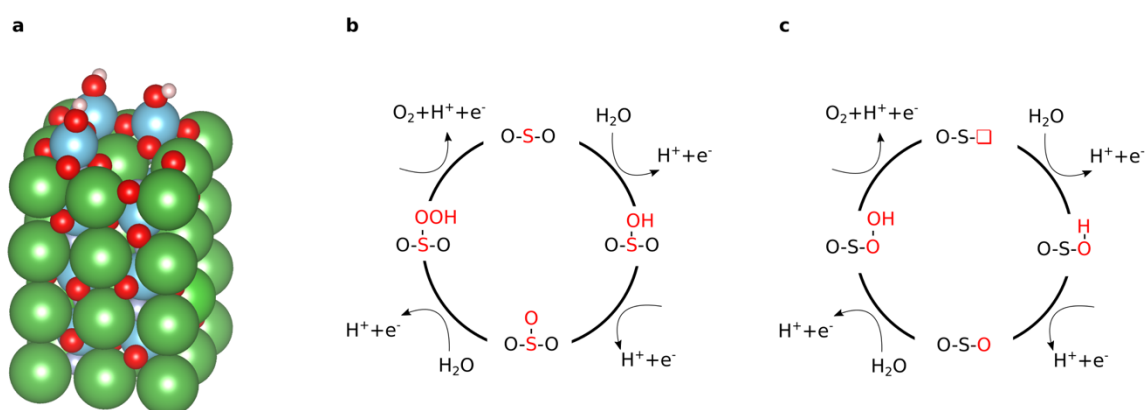


Figure 1 Surface structure example and catalytic cycles. **a**, Example of a *trans* LaTiO₂N slab with one Ti vacancy and the Ti atoms in the top layer covered with OH. Colour code: La = green, Ti = blue, O = red, H = white. **b**, Conventional OER reaction mechanisms considered and **c**, OER mechanism involving lattice oxygen.

We consider here only the conventional OER mechanism of four PCET steps (see equation 1-4) that is depicted in figure 1b) as we want to study the influence of different reaction sites irrespective of the reaction mechanism. This conventional mechanism does normally not include oxygen ions that are part of the slab. However, in the vicinity

of defects and adsorbates it is not always clear if an oxygen originated as part of the adsorbate or the slab and whether the conventional mechanism depicted in figure 1b can be applied or not. Therefore, we also include the OER mechanism shown in Figure 1c which is mathematically equivalent to the conventional mechanism shown in Figure 1b but operates on an oxygen deficient surface. This so-called lattice oxygen evolution²⁰ was experimentally observed²¹⁻²³ and also explained by basic thermodynamic concepts²⁴. Alternative lattice oxygen evolution mechanisms have been proposed^{25,26}, which are however mathematically different from the conventional mechanism (equations 1-4) and were therefore not included in this study.

In total we calculate the OER on 770 symmetrically inequivalent reaction sites (327 *trans* LTON, 135 *cis* LTON, 176 STO, 132 SRO) on 106 LTON, 35 STO and 39 SRO defective (001) surface models. The larger number of reaction sites on the oxynitride stems from anion-induced symmetry breaking. For roughly two thirds of the reaction sites either the *OOH or *OH intermediate was not stable and we exclude these cases from our analysis.

We calculate the change in free energy (ΔG) of the four reaction steps (1)-(4) using the computational standard hydrogen electrode (SHE)²⁷, where the energy of a proton and an electron equals half the energy of a hydrogen molecule. As the theoretical overpotential is not dependent on the pH or the potential² we perform our calculations at standard conditions (pH=0, T=298.15 K) and U=0 V. Zero-point energies (*ZPE*) and entropies (*S*) of the reaction intermediates were included as detailed elsewhere²⁸. In contrast to other studies, where *ZPE* was calculated for reaction intermediates in different environments (bridge vs. top site)²⁸, we always use the *ZPE* at the top site.

Given that for defective surfaces a full *ZPE* evaluation would be computationally prohibitively expensive and that previously reported changes in *ZPE* were minor²⁸, this approach will yield correct trends for defective surfaces.

We estimate the activity of a specific reaction site by the largest step in its OER free energy profile:

$$\Delta G^{OER} = \max[\Delta G_1^0, \Delta G_2^0, \Delta G_3^0, \Delta G_4^0] \quad (6)$$

ΔG_{1-4}^0 being the change in free energy of the four OER steps (equations 1–4). The calculated overpotential is given by:

$$\eta^{OER} = \frac{\Delta G^{OER}}{e} - 1.23 \text{ V} \quad (7)$$

where 1.23 V is the potential needed to make all ΔG s equal to zero for an ideal catalyst.

The adsorption free energies of the intermediate species ΔG_O , ΔG_{OH} and ΔG_{OOH} were calculated as follows:

$$\Delta G_{ads} = G_{ads+slab} - G_{slab} - nG_{H_2O} - mG_{H_2} \quad (8)$$

where free energies include changes in *ZPE* and *S* while *n* and *m* are stoichiometric coefficients that preserve the number of atoms on both sides of the respective reaction.

We further compare the calculated overpotential η^{OER} with the overpotential η_{UD}^{OER} predicted by the unique descriptor ΔG_2^0 : It was established that there exists a universal scaling relation between the adsorption energies of the reaction intermediates *OH and *OOH, their difference being approximately 3.2 eV for metal and oxide surfaces irrespective of the reaction site²⁹. Since the overpotential for oxides and metals is generally determined by either step 2 (ΔG_2^0) or 3 ($\Delta G_3^0 = 3.2 \text{ eV} - \Delta G_2^0$), the former is

often a suitable unique descriptor of the OER activity that determines the overpotential²:

$$\eta_{UD}^{OER} = \frac{\max[\Delta G_2^0, 3.2 \text{ eV} - \Delta G_2^0]}{e} - 1.23 \text{ V}, \quad (9)$$

where ΔG_2^0 is obtained via the difference in adsorption energies.

$$\Delta G_2^0 = \Delta G_O - \Delta G_{OH} \quad (10)$$

Under the assumption of an optimal $\Delta G_2^0 = \Delta G_3^0 = \frac{1}{2} 3.2 \text{ eV} = 1.6 \text{ eV}$, one arrives at a minimum possible overpotential of $\frac{1.6 \text{ eV}}{e} - 1.23 \text{ V} = 0.37 \text{ V}$. Deviations of ΔG_2^0 from this ideal value lead to larger unique-descriptor overpotentials.

Computational details

We determine energies of the various adsorbate covered, defective surfaces by density functional theory (DFT) calculations using the Quantum ESPRESSO³⁰ package at the GGA+U level of theory with the PBE³¹ exchange-correlation functional and a Hubbard U³² of 3 eV applied to the titanium 3*d* states. We do not apply a Hubbard U on ruthenium 4*d* orbitals as this setup results in the best agreements with experimentally measured magnetic moments and the density of states at the Fermi energy. We use ultrasoft pseudopotentials³³ with La(5*s*,5*p*,5*d*,6*s*), Sr(4*s*,4*p*,5*s*), Ti(3*s*,3*p*,3*d*,4*s*), Ru(4*d*,5*s*,5*p*), O(2*s*,2*p*) and N(2*s*,2*p*) electrons as valence states to describe the interaction between electrons and nuclei and perform spin-polarized calculations in the case of SrRuO₃. The cutoff for the plane-wave basis set is 40 Ry and 320 Ry for the kinetic energy and the augmented density respectively for LaTiO₂N

and SrTiO₃, while for SrRuO₃ we use slightly higher cutoffs of 50 Ry and 500 Ry respectively. We start our calculation from a 40-atom pseudo-cubic perovskite cell and create asymmetric 1x1x2 (001) surface slabs (see Figure 1a) with at least 10 Å vacuum, two fixed atomic layers at the bottom of the slab and a dipole correction in the vacuum layer³⁴. The Brillouin zone is sampled with a 4x4x1 Monkhorst-Pack³⁵ k-point grid for LaTiO₂N and SrTiO₃ and a 6x6x1 grid for SrRuO₃. We relax ionic position until forces converge below 0.05 eVÅ⁻¹ and total energies change by less than 1.4·10⁻⁵ eV.

Results and Discussion

We begin our analysis by comparing the calculated overpotentials η^{OER} with the overpotential determined via the unique descriptor η_{UD}^{OER} and find in general a good agreement for the majority of the calculated overpotentials (see Figure 2a).

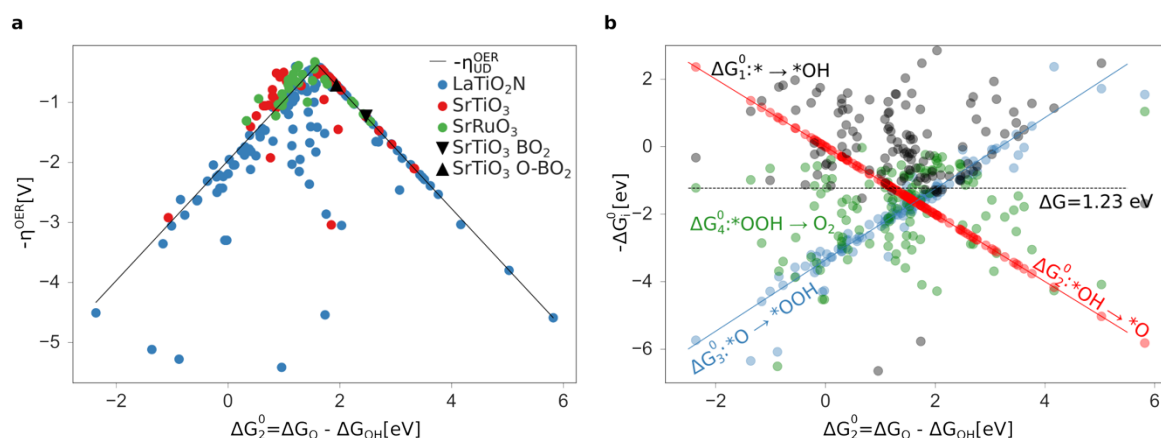


Figure 2 Volcano plot of defective surfaces and analysis of scaling relations of the oxynitride. **a**, Computed OER overpotential for defective LaTiO_2N , SrRuO_3 and SrTiO_3 surfaces plotted against the unique descriptor ΔG_2^0 , showing the usual volcano shape. For SrTiO_3 , we also show the overpotential for the bare (BO_2) and oxidised (O-BO_2) terminations. **b**, Dependence of the negative free energy change of the four OER steps on the unique descriptor ΔG_2^0 for LaTiO_2N . The difference between the horizontal $\Delta G = 1.23$ eV line and the lowest of the four negative reaction energies of a specific OER represents the predicted overpotential. The best linear fit for $-\Delta G_3^0$ is $1.05\Delta G_2^0 - 3.36$ ($R=0.91$, $\text{RSME} = 0.64$ eV), which is a slight deviation with respect to the scaling law that assumes a slope of 1 and an offset of 3.2 eV.

Most remarkable is the fact that we find for all three materials a continuous distribution of overpotentials within a large range of the unique descriptor ΔG_2^0 , including also the top of the volcano. While we cannot say, which sites (if any) will be predominantly present on a dissolving surface, it seems likely from the large number of sites close to

the minimum overpotential, that some of these will at least be transiently present. Since we omitted combinations of different defects types and only considered zero or full adsorbate coverage, the actual variety of reaction sites should be even larger. Together with alternative reaction mechanisms that could be active, we thus expect even more sites with small overpotentials on a metastable catalyst. It was reported that a relatively small number of highly active sites can dominate the apparent activity^{36,37}. We therefore postulate that in operando, surface dissolution can lead to the appearance of highly active sites, resulting in an enhanced apparent activity of the catalyst. In other words, the less a material is stable, the higher should be the diversity of reaction sites and the higher the chance of finding highly active reaction sites.

While previous studies³⁻⁵ suggest that active dissolution of the material results in the best activities, our results suggest that an activity enhancement can be achieved by an initial dissolution (preconditioning) that creates the variety of reaction sites but that the dissolution does not have to continue for high OER activities. This agrees with recent experimental findings for RuO₂ thin films, which show that while the surface orientation with the initially highest dissolution rate results in the best activities, an ongoing dissolution is not necessary for highly active surfaces⁶. It was also reported that the binding energy of reaction intermediates is not a good descriptor for the activity of metastable materials⁵. Our results suggest, however, that the large variation in binding energies for different reaction sites on the same metastable material can still explain the increase in activity on the basis of the adsorbate binding energies.

The similarity of the overpotential distribution of LTON, SRO and STO implies further that the high activity does not originate purely from the electronic structure of the

catalyst as is often assumed, but that reaction sites with geometries that enable a lower overpotential can form on any of the investigated materials. This is supported by the experimental finding that perovskite oxide electrocatalysts with structural flexibility can lead to superior activity³⁸. We want to stress that the proposed activity improvement requires the material to be metastable. As such, we do not expect a similar enhancement for the stable STO, where activities of the stoichiometric surfaces as indicated by black triangles in Figure 2a should prevail. Also, metastable materials such as LTON and SRO can of course only benefit from this proposed activity enhancement if the dissolution is slow enough for the material to still sustain extended periods of operation.

We continue by predicting the minimum overpotentials of the three materials. From the relation between the adsorption energies of the *OH and *OOH intermediates, we predict minimum overpotentials of 0.23 V for STO, 0.26 V for SRO and 0.40 V for LTON, the two former being slightly smaller than the 0.37 V predicted by the scaling relations, while the latter is slightly larger. Despite these differences, we do for STO and SRO not find actual reaction sites with overpotentials smaller than 0.37 V. This is in line with the observation that breaking the universal scaling relation between *OOH and *OH is a necessary but not sufficient condition to optimize the OER³⁹. Further, while there are only small differences between the two oxides that show a rather good agreement between the calculated η^{OER} and the unique-descriptor overpotentials η_{UD}^{OER} , for LTON we find a not insignificant number of reaction sites that show large deviations from η_{UD}^{OER} . A more detailed analysis of the reaction free energies of the four charge transfer steps ΔG_i^0 for LTON (see Figure 2b), reveals that while for most reactions ΔG_2^0 or ΔG_3^0 (blue and red data points) have the largest free-energy change,

there are some reactions where ΔG_4^0 (green data points) has the largest free energy change and is the limiting step. This implies that for the oxynitride the step from *OOH to O₂ is energetically less favourable while at the same time the formation of *OH is more favourable. This difference with respect to oxides² suggests a stronger adsorption of *OOH on the oxynitride and leads to larger calculated overpotentials compared to the unique-descriptor overpotentials η_{UD}^{OER} for some of the OERs.

From the volcano plot in Figure 2a we can see a further difference between the two oxides and the oxynitride: While for the oxynitride the descriptor value ΔG_2^0 ranges from -2 eV to 6 eV, the two oxides seem to have a much smaller range of ΔG_2^0 and their overpotentials are therefore more concentrated around the top of the volcano. The spread in ΔG_2^0 is important for the apparent activity. A catalyst with an activity of the perfect surface far from the top of the volcano would benefit from a large spread to increase the number of highly active sites. An already good catalyst located not far from the top of the volcano, on the other hand, would benefit from a small spread to have a large proportion of highly active sites. By looking for material parameters that determine and explain the range of the descriptor ΔG_2^0 , we fail to identify single structural features (such as e.g. reaction site species, angles and bond lengths of reaction intermediates or the adsorbate coverages to mention only a few). We also find no correlation of ΔG_2^0 with global properties such as the dipole moment of the slab or the nominal charge of the atoms. However, in agreement with other studies^{40,41}, we observe a correlation of ΔG_2^0 with the electronic structure. To characterize the charge transfer towards different reaction intermediates we look at the average Löwdin charges⁴² of the anions. We find the best correlations if we include all anions and not

only surface atoms. We compute differences between element-averaged Löwdin charges for the different reaction steps:

$$\Delta L_a^{i-j} = \frac{1}{N_a^i} \sum_{x \in a} l_x^i - \frac{1}{N_a^j} \sum_{x \in a} l_x^j \quad (5)$$

where a is an anion (here O or N), i and j are two consecutive reaction intermediates, $N_a^{i/j}$ is the number of a atoms in the surface structure with the i/j intermediate and $l_x^{i/j}$ is the Löwdin charge for atom x in the structure with intermediate i/j , while the sum runs over all atoms of element a .

As we show in Figure 3a, there is a direct correlation between the descriptor ΔG_2^0 and the average change in Löwdin charge of the oxygen ions ΔL_O^{*OH-*O} for LTON. We do, however, not see a correlation for STO or SRO, which may be related to the smaller range of ΔG_2^0 for these materials. ΔL_O^{*OH-*O} is generally positive, meaning that the average Löwdin charge of oxygen is higher for the OH* than for the O* intermediate, which we can relate to the fact that oxygen in *OH attracts electrons from the hydrogen atom and the slab whereas *O attracts electrons only from the slab. A smaller ΔL_O^{*OH-*O} signifies less charge transfer from the slab to the adsorbate during deprotonation, implying that both adsorbates attract a similar number of electrons, which results in an energetically more favourable deprotonation and a smaller ΔG_2^0 , giving a physical interpretation to the correlation in Figure 3a.

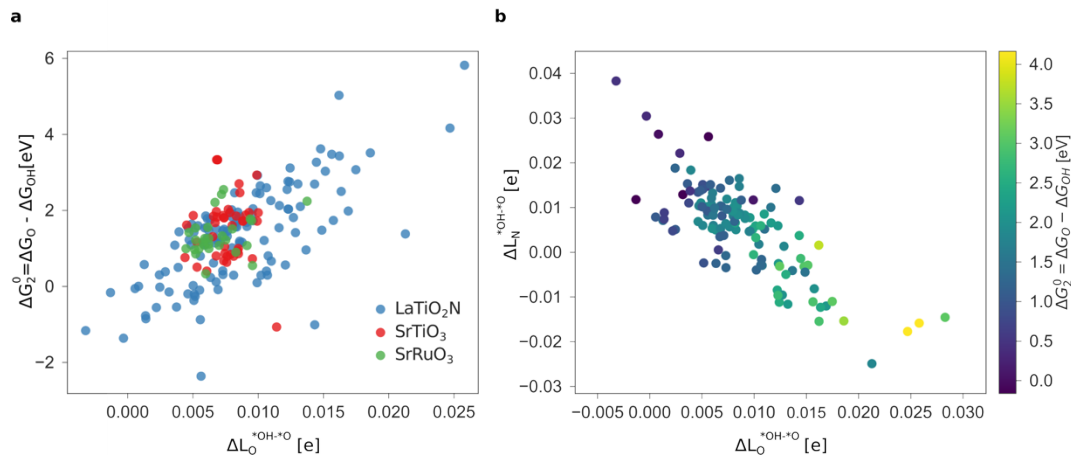


Figure 3 Charge-transfer effects on electrochemistry. **a**, Correlation between the change in Löwdin charge ΔL_O^{*OH-*O} on oxygen and the unique descriptor ΔG_2^0 . Larger L_O^{*OH-*O} indicate that the oxygen atoms lose more electrons when the reaction intermediate changes from $*OH$ to $*O$. This is energetically costly and results in large free energy changes ΔG_2^0 . **b**, Correlation between the change in Löwdin charge ΔL_O^{*OH-*O} on oxygen and ΔL_N^{*OH-*O} on nitrogen. The colour bar indicates the value of the descriptor ΔG_2^0 .

For the oxides SRO and STO the range of ΔL_O^{*OH-*O} is much smaller than for LTON leading to a smaller range in ΔG_2^0 . We can explain this difference between oxides and oxynitrides by relating the average change in Löwdin charge of oxygen ΔL_O^{*OH-*O} to the one of nitrogen ΔL_N^{*OH-*O} . As shown in Figure 3b we find an inverse correlation between these charge differences, suggesting a charge transfer from N to O. From the colour coding of the data points, we see that ΔG_2^0 is generally smaller when nitrogen loses more electrons (large positive ΔL_N^{*OH-*O}), while the charge variation on the oxygen atoms is small. From these observations we propose that nitrogen can act as an electron reservoir: The reaction from $*OH$ to $*O$ is favoured if nitrogen ions provide electrons, resulting in a lower descriptor value ΔG_2^0 , while reaction sites, where

this charge transfer is not possible, result in larger ΔG_2^0 s. More generally, this implies that a more flexible valence-band electronic structure, for example in mixed-anion materials, can yield a larger variety of ΔG_2^0 s and thus potentially an increased apparent activity.

While for the oxynitride we find a correlation of ΔG_2^0 with the change in Löwdin charges, using this change to predict ΔG_2^0 would result in relatively large errors (RSME = 0.89 eV). Conventionally used descriptors such as d- or p-band centres^{10,43} were unable to predict ΔG_2^0 with a satisfactory accuracy also for the oxides. This suggests that finding descriptors for different reaction site geometries on defective surfaces of the same material is significantly more challenging than finding descriptors for the same perfect surface of different materials. Finding suitable descriptors for defective surfaces and determining common structural features of reaction sites at the top of the activity volcano will thus likely require advanced methods such as statistical learning, which can combine multiple descriptors. A detailed analysis of the different reaction sites and their corresponding activities is ongoing and will be presented in a follow-up paper.

Conclusions

In summary, we have shown for three electronically different perovskite materials that the structural variety of reaction sites on dissolving heterogeneous catalysts will, for some sites, lead to overpotentials close to the top of the activity volcano. Under the assumption that reaction sites with low overpotentials will dominate the apparent activity, this implies that independent of the electronic properties, operating a heterogeneous catalyst at the border of its stability region or preconditioning the

catalyst under metastable conditions can lead to an increased apparent activity due to the increased variety of geometrically different reaction sites. While we find the unique-descriptor approach to generally work well for these highly defective surfaces, we observe that the strong binding of the *OOH and *OH intermediates on LaTiO₂N can lead to different limiting steps and larger deviations from the descriptor-based overpotential than for oxides. The observed large spread in overpotentials for just a single reaction mechanism implies that assigning a computed mechanism based on agreement with experimentally measured overpotentials without detailed mechanistic studies is, despite being common practice, highly questionable. We find only minor differences in activity between metallic SrRuO₃ and insulating SrTiO₃ but show that a flexible valence band structure as it occurs in LaTiO₂N yields a larger variety of ΔG_2^0 values.

Acknowledgements

This research was funded by the SNF Professorship Grant PP00P2_157615. Calculations were performed on UBELIX (<http://www.id.unibe.ch/hpc>), the HPC cluster at the University of Bern, the Swiss National Supercomputing Centre (CSCS) under project s766 and SuperMUC at GCS@LRZ, Germany, for which we acknowledge PRACE for awarding us access.

References

- (1) Rossmeisl, J.; Logadottir, A.; Nørskov, J. K. Electrolysis of Water on (Oxidized) Metal Surfaces. *Chem. Phys.* **2005**, *319* (1–3), 178–184.

- (2) Man, I. C.; Su, H.-Y.; Calle-Vallejo, F.; Hansen, H. A.; Martinez, J. I.; Inoglu, N. G.; Kitchin, J.; Jaramillo, T. F.; Nørskov, J. K.; Rossmeisl, J. Universality in Oxygen Evolution Electrocatalysis on Oxide Surfaces. *ChemCatChem* **2011**, *3* (7), 1159–1165.
- (3) Chang, S. H.; Connell, J. G.; Danilovic, N.; Subbaraman, R.; Chang, K.-C.; Stamenkovic, V. R.; Markovic, N. M. Activity–Stability Relationship in the Surface Electrochemistry of the Oxygen Evolution Reaction. *Faraday Discuss.* **2014**, *176*, 125–133.
- (4) Danilovic, N.; Subbaraman, R.; Chang, K.-C.; Chang, S. H.; Kang, Y. J.; Snyder, J.; Paulikas, A. P.; Strmcnik, D.; Kim, Y.-T.; Myers, D.; et al. Activity–Stability Trends for the Oxygen Evolution Reaction on Monometallic Oxides in Acidic Environments. *J. Phys. Chem. Lett.* **2014**, *5* (14), 2474–2478.
- (5) Chang, S. H.; Danilovic, N.; Chang, K.-C.; Subbaraman, R.; Paulikas, A. P.; Fong, D. D.; Highland, M. J.; Baldo, P. M.; Stamenkovic, V. R.; Freeland, J. W.; et al. Functional Links between Stability and Reactivity of Strontium Ruthenate Single Crystals during Oxygen Evolution. *Nat. Commun.* **2014**, *5*, 4191.
- (6) Roy, C.; Rao, R. R.; Stoerzinger, K. A.; Hwang, J.; Rossmeisl, J.; Chorkendorff, I.; Shao-Horn, Y.; Stephens, I. E. L. Trends in Activity and Dissolution on RuO₂ under Oxygen Evolution Conditions: Particles versus Well-Defined Extended Surfaces. *ACS Energy Lett.* **2018**, *3* (9), 2045–2051.
- (7) Rong, X.; Kolpak, A. M. Ab Initio Approach for Prediction of Oxide Surface Structure, Stoichiometry, and Electrocatalytic Activity in Aqueous Solution. *J. Phys. Chem. Lett.* **2015**, *6* (9), 1785–1789.
- (8) Kim, B.-J.; Abbott, D. F.; Cheng, X.; Fabbri, E.; Nachttegaal, M.; Bozza, F.; Castelli, I. E.; Lebedev, D.; Schäublin, R.; Copéret, C.; et al. Unraveling Thermodynamics, Stability, and Oxygen Evolution Activity of Strontium Ruthenium Perovskite Oxide. *ACS Catal.* **2017**, *7* (5), 3245–3256.
- (9) Singh, A. K.; Zhou, L.; Shinde, A.; Suram, S. K.; Montoya, J. H.; Winston, D.; Gregoire, J. M.; Persson, K. A. Electrochemical Stability of Metastable Materials. *Chem. Mater.* **2017**, *29* (23), 10159–10167.
- (10) Montoya, J. H.; Doyle, A. D.; Nørskov, J. K.; Vojvodic, A. Trends in Adsorption of Electrocatalytic Water Splitting Intermediates on Cubic ABO₃ Oxides. *Phys. Chem. Chem. Phys.* **2018**, *20* (5), 3813–3818.
- (11) Montoya, J. H.; Garcia-Mota, M.; Nørskov, J. K.; Vojvodic, A. Theoretical Evaluation of the Surface Electrochemistry of Perovskites with Promising Photon Absorption Properties for Solar Water Splitting. *Phys. Chem. Chem. Phys.* **2015**, *17* (4), 2634–2640.
- (12) Dickens, C. F.; Nørskov, J. K. A Theoretical Investigation into the Role of Surface Defects for Oxygen Evolution on RuO₂. *J. Phys. Chem. C* **2017**, *121* (34), 18516–18524.
- (13) Dickens, C. F.; Montoya, J. H.; Kulkarni, A. R.; Bajdich, M.; Nørskov, J. K. An Electronic Structure Descriptor for Oxygen Reactivity at Metal and Metal-Oxide

- Surfaces. *Surf. Sci.* **2019**, *681*, 122–129.
- (14) Kasahara, A.; Nukumizu, K.; Takata, T.; Kondo, J. N.; Hara, M.; Kobayashi, H.; Domen, K. LaTiO₂N as a Visible-Light (≤ 600 nm)-Driven Photocatalyst. *J. Phys. Chem. B* **2003**, *107* (3), 791–797.
 - (15) Castelli, I. E.; Thygesen, K. S.; Jacobsen, K. W. Calculated Pourbaix Diagrams of Cubic Perovskites for Water Splitting: Stability against Corrosion. *Top. Catal.* **2014**, *57* (1–4), 265–272.
 - (16) Kasahara, A.; Nukumizu, K.; Hitoki, G.; Takata, T.; Kondo, J. N.; Hara, M.; Kobayashi, H.; Domen, K. Photoreactions on LaTiO₂N under Visible Light Irradiation. *J. Phys. Chem. A* **2002**, *106*, 6750–6753.
 - (17) Yang, M.; Oró-Solé, J.; Rodgers, J. A.; Jorge, A. B.; Fuertes, A.; Atfield, J. P. Anion Order in Perovskite Oxynitrides. *Nat. Chem.* **2011**, *3* (1), 47–52.
 - (18) Ninova, S.; Aschauer, U. Surface Structure and Anion Order of the Oxynitride LaTiO₂N. *J. Mater. Chem. A* **2017**, *5* (22), 11040–11046.
 - (19) Ninova, S.; Aschauer, U. Anion-Order Driven Polar Interfaces at LaTiO₂N Surfaces. *J. Mater. Chem. A* **2019**, *7* (5), 2129–2134.
 - (20) Fabbri, E.; Schmidt, T. J. Oxygen Evolution Reaction - the Enigma in Water Electrolysis. *ACS Catal.* **2018**, *8* (10), 9765–9774.
 - (21) Wohlfahrt-Mehrens, M.; Heitbaum, J. Oxygen Evolution on Ru and RuO₂ Electrodes Studied Using Isotope Labelling and on-Line Mass Spectrometry. *J. Electroanal. Chem. interfacial Electrochem.* **1987**, *237* (2), 251–260.
 - (22) Fierro, S.; Nagel, T.; Baltruschat, H.; Comninellis, C. Investigation of the Oxygen Evolution Reaction on Ti/IrO₂ Electrodes Using Isotope Labelling and on-Line Mass Spectrometry. *Electrochem. commun.* **2007**, *9* (8), 1969–1974.
 - (23) Diaz-Morales, O.; Calle-Vallejo, F.; de Munck, C.; Koper, M. T. M. Electrochemical Water Splitting by Gold: Evidence for an Oxide Decomposition Mechanism. *Chem. Sci.* **2013**, *4* (6), 2334–2343.
 - (24) Binninger, T.; Mohamed, R.; Waltar, K.; Fabbri, E.; Levecque, P.; Kötz, R.; Schmidt, T. J. Thermodynamic Explanation of the Universal Correlation between Oxygen Evolution Activity and Corrosion of Oxide Catalysts. *Sci. Rep.* **2015**, *5*, 12167.
 - (25) Grimaud, A.; Diaz-Morales, O.; Han, B.; Hong, W. T.; Lee, Y.-L.; Giordano, L.; Stoerzinger, K. A.; Koper, M. T. M.; Shao-Horn, Y. Activating Lattice Oxygen Redox Reactions in Metal Oxides to Catalyse Oxygen Evolution. *Nat. Chem.* **2017**, *9* (5), 457–465.
 - (26) Yoo, J. S.; Rong, X.; Liu, Y.; Kolpak, A. M. Role of Lattice Oxygen Participation in Understanding Trends in the Oxygen Evolution Reaction on Perovskites. *ACS Catal.* **2018**, *8* (5), 4628–4636.
 - (27) Nørskov, J. K.; Rossmeisl, J.; Logadottir, A.; Lindqvist, L.; Kitchin, J. R.; Bligaard, T.; Jonsson, H. Origin of the Overpotential for Oxygen Reduction at a Fuel-Cell Cathode. *J. Phys. Chem. B* **2004**, *108* (46), 17886–17892.
 - (28) Valdés, Á.; Qu, Z.-W.; Kroes, G.-J.; Rossmeisl, J.; Nørskov, J. K. Oxidation

- and Photo-Oxidation of Water on TiO₂ Surface. *J. Phys. Chem. C* **2008**, *112* (26), 9872–9879.
- (29) Koper, M. T. M. Thermodynamic Theory of Multi-Electron Transfer Reactions: Implications for Electrocatalysis. *J. Electroanal. Chem.* **2011**, *660* (2), 254–260.
- (30) Giannozzi, P.; Baroni, S.; Bonini, N.; Calandra, M.; Car, R.; Cavazzoni, C.; Ceresoli, D.; Chiarotti, G. L.; Cococcioni, M.; Dabo, I.; et al. QUANTUM ESPRESSO: A Modular and Open-Source Software Project for Quantum Simulations of Materials. *J. Phys. Condens. Matter* **2009**, *21* (39), 395502.
- (31) Perdew, J. P.; Burke, K.; Ernzerhof, M. Generalized Gradient Approximation Made Simple. *Phys. Rev. Lett.* **1996**, *77* (18), 3865–3868.
- (32) Anisimov, V. I.; Zaanen, J.; Andersen, O. K. Band Theory and Mott Insulators: Hubbard U Instead of Stoner I. *Phys. Rev. B* **1991**, *44* (3), 943–954.
- (33) Vanderbilt, D. Soft Self-Consistent Pseudopotentials in a Generalized Eigenvalue Formalism. *Phys. Rev. B* **1990**, *41* (11), 7892–7895.
- (34) Bengtsson, L. Dipole Correction for Surface Supercell Calculations. *Phys. Rev. B* **1999**, *59* (19), 12301.
- (35) Monkhorst, H. J.; Pack, J. D. Special Points for Brillouin-Zone Integrations. *Phys. Rev. B* **1976**, *13* (12), 5188–5192.
- (36) Sun, G.; Sautet, P. Metastable Structures in Cluster Catalysis from First-Principles: Structural Ensemble in Reaction Conditions and Metastability Triggered Reactivity. *J. Am. Chem. Soc.* **2018**, *140* (8), 2812–2820.
- (37) Batchelor, T. A. A.; Pedersen, J. K.; Winther, S. H.; Castelli, I. E.; Jacobsen, K. W.; Rossmeisl, J. High-Entropy Alloys as a Discovery Platform for Electrocatalysis. *Joule* **2019**, *in press*.
- (38) Fabbri, E.; Nachtegaal, M.; Binniger, T.; Cheng, X.; Kim, B.-J.; Durst, J.; Bozza, F.; Graule, T.; Schäublin, R.; Wiles, L.; et al. Dynamic Surface Self-Reconstruction Is the Key of Highly Active Perovskite Nano-Electrocatalysts for Water Splitting. *Nat. Mater.* **2017**, *6*, 8106–8108.
- (39) Govindarajan, N.; Garcia-Lastra, J. M.; Meijer, E. J.; Calle-Vallejo, F. Does the Breaking of Adsorption-Energy Scaling Relations Guarantee Enhanced Electrocatalysis? *Curr. Opin. Electrochem.* **2018**.
- (40) Vojvodic, A.; Nørskov, J. K. Optimizing Perovskites for the Water-Splitting Reaction. *Science* **2011**, *334* (6061), 1355–1356.
- (41) Nørskov, J. K.; Abild-Pedersen, F.; Studt, F.; Bligaard, T. Density Functional Theory in Surface Chemistry and Catalysis. *PNAS* **2011**, *108* (3), 937–943.
- (42) Lowdin, P. O. On the Non-Orthogonality Problem Connected with the Use of Atomic Wave Functions in the Theory of Molecules and Crystals. *J. Chem. Phys.* **1950**, *18* (3), 365–375.
- (43) Hammer, B.; Nørskov, J. K. Why Gold Is the Noblest of All the Metals. *Nature* **1995**, *376* (6537), 238–240.

